Remote Sensing in Ecology and Conservation
Open Access
ZSL

RESEARCH ARTICLE

Uncovering mangrove range limits using very high resolution satellite imagery to detect fine-scale mangrove and saltmarsh habitats in dynamic coastal ecotones

Cheryl L. Doughty[1,2,3], Kyle C. Cavanaugh[4], Samantha Chapman[5] & Lola Fatoyinbo[1]

[1]Biospheric Sciences Laboratory, NASA Goddard Space Flight Center, Greenbelt Maryland, 20771, USA
[2]Oak Ridge Associated Universities, Oak Ridge Tennessee, 37831, USA
[3]Earth System Science Interdisciplinary Center, University of Maryland, College Park Maryland, 20740, USA
[4]Department of Geography, University of California, Los Angeles California, 90095, USA
[5]Department of Biology and Center for Biodiversity and Ecosystem Stewardship, Villanova University, Villanova Pennsylvania, 19085, USA

Keywords
Coastal wetland, global climate change, landcover classification, mangroves, random forest, WorldView

Correspondence
Cheryl L. Doughty, Biospheric Sciences Laboratory, NASA Goddard Space Flight Center, Greenbelt, MD 20771, USA. E-mail: cheryl.l.doughty@nasa.gov

Funding information
This research was supported by the NASA Postdoctoral Program Fellowship awarded to Cheryl Doughty and administered by Oak Ridge Associated Universities. This research was also supported by the National Aeronautics and Space Administration (NASA) Land Use/Land Cover Change Program (grant number WBS437949.02.06.01.36).

Editor: Prof. Mat Disney
Associate Editor: Dr. Alice Jones

Received: 21 December 2023; Revised: 9 March 2024; Accepted: 3 April 2024

doi: 10.1002/rse2.394

Abstract

Mangroves are important ecosystems for coastal biodiversity, resilience and carbon dynamics that are being threatened globally by human pressures and the impacts of climate change. Yet, at several geographic range limits in tropical–temperate transition zones, mangrove ecosystems are expanding poleward in response to changing macroclimatic drivers. Mangroves near range limits often grow to smaller statures and form dynamic, patchy distributions with other coastal habitats, which are difficult to map using moderate-resolution (30-m) satellite imagery. As a result, many of these mangrove areas are missing in global distribution maps. To better map small, scrub mangroves, we tested Landsat (30-m) and Sentinel (10-m) against very high resolution (VHR) Planet (3-m) and WorldView (1.8-m) imagery and assessed the accuracy of machine learning classification approaches in discerning current (2022) mangrove and saltmarsh from other coastal habitats in a rapidly changing ecotone along the east coast of Florida, USA. Our aim is to (1) quantify the mappable differences in landscape composition and complexity, class dominance and spatial properties of mangrove and saltmarsh patches due to image resolution; and (2) to resolve mapping uncertainties in the region. We found that the ability of Landsat to map mangrove distributions at the leading range edge was hampered by the size and extent of mangrove stands being too small for detection (50% accuracy). WorldView was the most successful in discerning mangroves from other wetland habitats (84% accuracy), closely followed by Planet (82%) and Sentinel (81%). With WorldView, we detected 800 ha of mangroves within the Florida range-limit study area, 35% more mangroves than were detected with Planet, 114% more than Sentinel and 537% more than Landsat. Higher-resolution imagery helped reveal additional variability in landscape metrics quantifying diversity, spatial configuration and connectedness among mangrove and saltmarsh habitats at the landscape, class and patch scales. Overall, VHR satellite imagery improved our ability to map mangroves at range limits and can help supplement moderate-resolution global distributions and outdated regional maps.

Introduction

Efforts to map mangroves across the world using remote sensing have provided incredible insights into global mangrove extents (Giri et al., 2011, Hamilton & Casey, 2016, Bunting et al., 2022), forest heights and biomass (Simard et al., 2019) and carbon storage (Sanderman et al., 2018). Such baselines of knowledge have

revealed where and why mangroves are being lost and degraded (Thomas et al., 2017, 2018; Goldberg et al., 2020; Bryan-Brown et al., 2020), and the consequences to important ecosystem functions like carbon storage and cycling (Richards et al., 2020; Adame et al., 2021). Similar efforts are also improving our understanding of saltmarsh extents, changes and impacts across the world (McOwen et al., 2017; Murray et al., 2019, 2022; Campbell et al., 2022). Yet, global maps derived from moderate-resolution satellite data have difficulty capturing coastal habitats that are small in extent, short in height and in regions experiencing disturbance or containing fragmented or fringe mangrove forests (Bunting et al., 2018; Simard et al., 2019).

At the latitudinal limits of their geographic ranges, tropical mangrove ecosystems converge with temperate or arid regions to form spatially and structurally unique transition zones between adjacent coastal habitats (Quisthoudt et al., 2012). Often referred to as 'ecotones', these areas represent a transitional gradient among two ecosystems, whereas a 'range limit' is the theoretical line delineating the existence of one ecosystem (Risser, 1995; Quisthoudt et al., 2012; Smith et al., 2013). Because mangroves in ecotonal regions are often at the limits of their physiological thresholds, their forms are typically shorter and more scrub like than in the tropics (Morrisey et al., 2010), and they are highly sensitive to environmental changes such as sea level rise, precipitation changes and freeze events (Osland et al., 2017). Ecotones represent gradients in macroclimatic drivers like temperature and precipitation in which small abiotic changes can result in large and abrupt differences in ecosystem structure (Osland et al., 2016). As a result, range-limit mangrove ecotones can be highly dynamic and form a heterogeneous mosaic with other coastal habitats at fine scales across the landscape. Detection of mangrove encroachment at coarse resolutions may be lagged as changes in habitat presence and abundance culminate into spectral changes over time. Recent warming trends have coincided with mangrove expansion into adjacent coastal saltmarshes in some regions across the world (Saintilan et al., 2014; Cavanaugh et al., 2014, 2018; Rodriguez et al., 2016). However, the limitations of global mapping efforts have led to large gaps and uncertainty in the areal extents and latitudinal limits of mangroves (Ximenes et al., 2022).

Ongoing advancements in Earth Observation (EO) have improved the spatial, temporal and spectral resolutions of remotely sensed data used to study wetland ecosystems (Klemas, 2011, 2013, 2015). As very high resolution (VHR; <5 m) satellite imagery becomes increasingly available, mapping accuracies have improved among wetland classes in smaller pixels better matched to the size of wetland features and therefore less spectrally mixed (McCarthy et al., 2015; Turpie et al., 2015; Davidson et al., 2018; Doughty & Cavanaugh, 2019; Doughty et al., 2021; Krause et al., 2023). VHR imagery and machine learning classification approaches have been combined in tropical mangrove sites to improve mapping on fine scales and provide high-resolution insights into habitat heterogeneity, structure and biomass (Kamal et al., 2014, 2015, 2022). The use of VHR imagery at mangrove range limits across the world could help reduce the current uncertainty in global extents and establish better baselines to assess wetland dynamics in relation to macroclimate drivers (Ximenes et al., 2022; Bardou et al., 2023).

The more habitat heterogeneity revealed with VHR, the greater the ecological insights into mangrove–saltmarsh ecotones. Landscape patterns can be used to describe the composition and configuration of habitats across a landscape, and these patterns can be related to ecological processes (Turner, 1990). Landscape metrics, for example, patch size or nearest-neighbor distance, provide a mechanism for quantifying the spatial patterns in landscapes that have an impact on ecosystem structure, function, biodiversity or services (Uuemaa et al., 2013; Turner & Gardner, 2015; Lausch et al., 2015). Measured over time, changes in landscape metrics can also dictate the rate of change and patchiness of impacts caused by climate drivers (Turner & Ruscher, 1988; López-Hoffman et al., 2013). However, landscape metrics are sensitive to resolution, scope, classification scheme and interpretation (Liu & Cameron, 2001; Lustig et al., 2015). In mangrove–saltmarsh ecotones, patterns at the patch scale have been shown to play a critical and differential role in propagule dispersal and seedling establishment dynamics, and such insights ultimately need to be scaled up to better understand range-limit dynamics (Yando et al., 2021). VHR imagery may provide the appropriate resolutions to help bridge the gap between the patch and the landscape and to help estimate landscape metrics at scales better matched to ecological properties than coarser-resolution imagery (Foody, 2023).

The east coast of Florida, USA, is one such range limit experiencing rapid climate-driven expansion of woody mangroves into herbaceous saltmarshes (Cavanaugh et al., 2014, 2018), where discrepancies exist among mapped distributions and observations from the field (Bardou et al., 2023). Here, mangrove encroachment can alter ecosystem services (Kelleway et al., 2017; Osland, Hughes, et al., 2022), with local impacts in the NE Florida region already documented for ecosystem carbon storage (Doughty et al., 2016; Simpson et al., 2019; Vaughn et al., 2020; Steinmuller et al., 2022), coastal protection (Doughty et al., 2017), soil processes and maintenance

(Coldren et al., 2019, Howard et al., 2020, Geoghegan et al., 2021, Simpson et al., 2021) and trophic interactions (Goeke et al., 2023). To truly understand the aggregate consequences to ecosystem structure and function at landscape and regional scales, ultimately, increased resolutions are needed to map mangrove extent and change on fine scales. Such improvements to mapping are still needed by coordinated monitoring networks aimed at managing rapidly changing coastal regions (Bardou et al., 2023).

To better map mangroves within range limits, we tested available satellite imagery ranging in spatial resolution from 1.8 to 30 m by applying machine learning approaches to classify current (2022) habitat distributions in the rapidly changing mangrove–saltmarsh ecotone along the east coast of Florida, USA. We compare commonly used Landsat (30 m) and Sentinel (10 m) with very-high-resolution (VHR) commercial Planet (3 m) and WorldView (1.8 m) imagery and assess the accuracy of discerning mangrove and saltmarsh from other coastal habitats. Our aim is to (1) quantify the mappable differences in landscape composition and complexity, class dominance and spatial properties of mangrove and saltmarsh patches due to image resolution and (2) to resolve mapping uncertainties in the region. Improved understanding of mangrove distributions within range limits will be vital for monitoring ongoing climate-driven changes at local scales and for reducing uncertainty in estimates of global mangrove drivers, carbon storage, and more derived from global maps.

Materials and Methods

Study area

Mangroves occupy 5 continents and there are 14 range-limit regions defined worldwide according to the geographic and macroclimatic constraints to distribution (Quisthoudt et al., 2012; Saintilan et al., 2014; Osland et al., 2017). For this study, we focused on the mangrove range limit in Eastern North America, where mangrove distributions in Florida, USA, have been expanding northward in recent decades (Cavanaugh et al., 2014). The three mangrove species present in the region, *Avicennia germinans*, *Rhizophora mangle* and *Laguncularia racemosa*, are distributed latitudinal by cold tolerance with *A. germinans* and *R. mangle* observed at the leading edge of the range limit. The bounds of the Florida range limit were informed by a comparison of global maps of mangroves (Global Mangrove Watch (GMW v3.0); Bunting et al., 2022) and saltmarshes (Global Map of Saltmarshes (GMS); McOwen et al., 2017), as well as published records of field observations. Within the range limit, we conducted our mapping analyses in a c. 1500 km^2 area at the leading edge of the range limit where imagery was available from all sensors (Fig. 1). This area includes the Guana Tolomato Matanzas National Estuarine Research Reserve (GTMNERR) that is home to a mosaic of estuarine habitats representing northeast Florida (Dix et al., 2021).

We limited our analyses to relevant coastal wetland areas by creating a coastal mask that combined previously mapped global distributions of mangroves (Bunting et al., 2022), salt marshes (McOwen et al., 2017), tidal flats (Murray et al., 2019) and coastal waters extracted from Hansen et al. (2013) at a spatial resolution of 30 m. We applied a closing morphological filter to remove gaps in the coastal mask that may correspond to adjacent wetland habitats occupying smaller scales (<30 m).

Satellite imagery sources and preprocessing

We selected cloud-free satellite images over the study area taken from single dates in January 2022 when seasonal differences in vegetation senescence are clear (Table S1). We chose to collect each image directly from their source institutions instead of downscaling a single VHR to lower resolutions as this can introduce and amplify mapping artifacts (Li & Wu, 2004), and because we wanted to test the inherent variability among the available imagery. Commercial WorldView and PlanetScope imagery are available for government research through the NextView License Agreement (Neigh et al., 2013) and NASA's Commercial Smallsat Data Acquisition (CSDA) Program (Maskey et al., 2021). WorldView-2 (WV2) imagery was obtained from MAXAR's Global Enhanced GEOINT Delivery portal as 16-bit basic multispectral (8-band) and pan images that are not georeferenced or calibrated. Images were orthorectified, radiometrically calibrated and mosaicked using the open-source Orfeo Toolbox (OTB; Grizonnet et al., 2017) plugin in QGIS (v3.28.2; QGIS Development Team, 2023). Radiometric calibration uses the 6S radiotransfer model parameterized with the image metadata to produce top-of-atmosphere (TOA) images which are then atmospherically corrected to top-of-canopy surface reflectance. Images were then mosaicked using band harmonization to create the WorldView scene defining the mapping AOI of our study (Fig. 1C). PlanetScope SuperDove imagery was accessed through the Planet Explorer. SuperDove, hereafter 'Planet', 8-band multispectral images were available for download as georeferenced, harmonized surface reflectance. Planet images were mosaicked using band harmonization in OTB to cover the study area.

Sentinel and Landsat imagery were accessed and preprocessed in Google Earth Engine (GEE), a cloud-based platform for storing and analyzing geospatial and

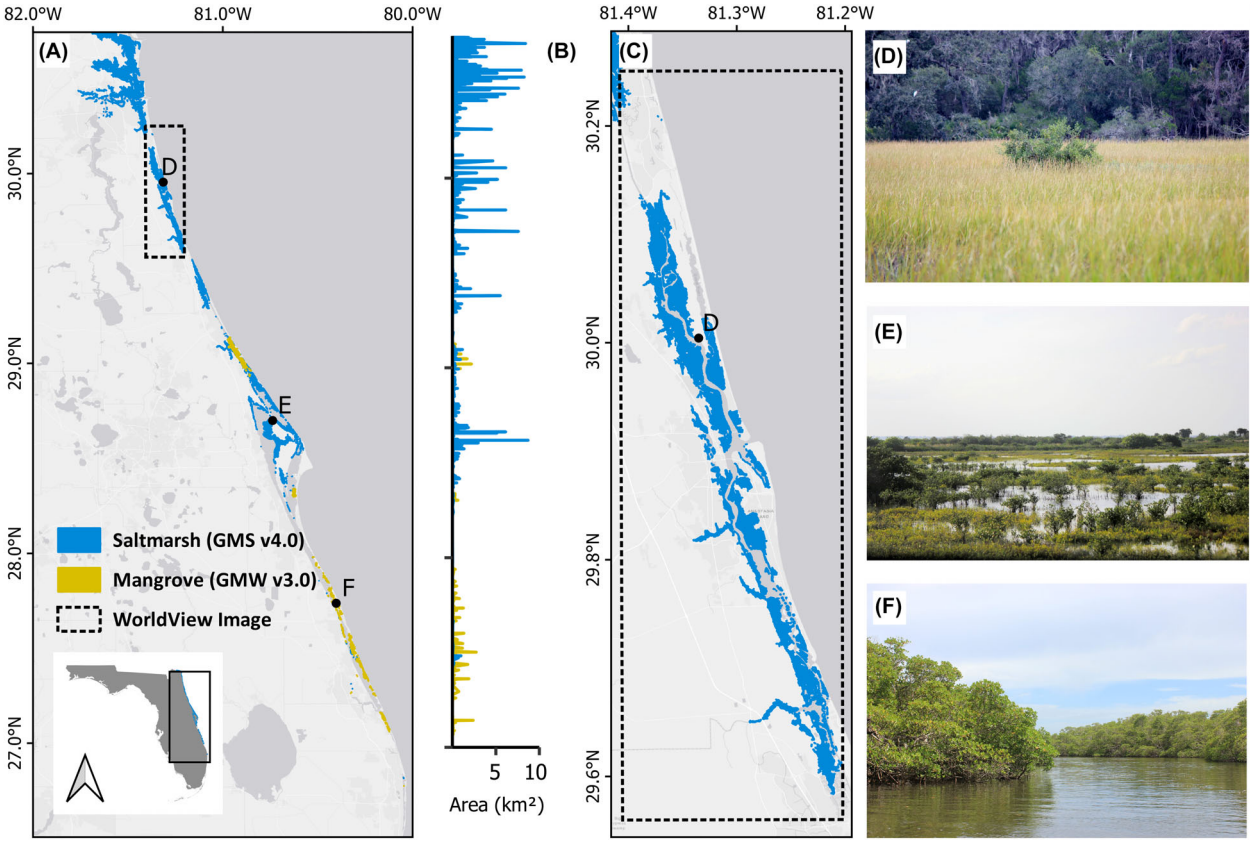

Figure 1. Coastal areas in (A) eastern Florida, USA, with global distributions of saltmarsh (blue; GMS v3.0; McOwen et al. 2017) and mangrove (yellow; GMW v3.0; Bunting et al. 2022), and (B) areas of each habitat along the latitudinal gradient. The (C) study area covered by the WorldView image (dashed line) with field photos (D–F) showing mangrove trees and stands within the ecotonal range limit.

remotely sensed data (Gorelick et al., 2017). We used the Sentinel-2 MultiSpectral Instrument (MSI) Level-1C TOA data and converted TOA to bottom-of-atmosphere (BOA) surface reflectance using the sensor invariant atmospheric correction (SIAC) method (Yin et al., 2019). Images were then mosaicked to cover the study area. Last, we used a NASA/USGS Landsat 8 OLI (Level 2, Collection 2 and Tier 1) scene available as atmospherically corrected surface reflectance in GEE to create multispectral 8-band mosaics coinciding with the study area.

We selected spectral bands available across all images and calculated indices that have proven useful in mangrove classification (Goldberg et al., 2020; Hickey & Radford, 2022; Tran et al., 2022). Vegetation indices included the normalized difference mangrove index (NDVI; Rouse et al., 1974), normalized difference water index (NDWI; McFeeters, 1996), simple ratio of red and near-infrared bands (SR) and the green chlorophyll vegetation index (GCVI). To differentiate non-vegetated pixels (water, bare) from vegetated pixels, we used a threshold of 0.2 for NDVI and NDWI when masking.

Classification and postprocessing

Training data

We created a vector training dataset to represent the relevant habitats in our study area for classification of all 2022 images. Training polygons were initially created within areas previously mapped globally as mangrove, saltmarsh, tidal mudflat and water (Bunting et al., 2022; McOwen et al., 2017; Murray et al., 2019; Hansen et al., 2013). We added previously unmapped mangrove areas to the mangrove training class, and for the purpose of this analysis, all mangrove species were grouped into a single class. We also added urban/built and upland vegetation classes to the training dataset based on the WorldView image. To ensure that training data could be used across all images ranging in resolution from 1.85 to 30 m, we visually checked all training polygons against the WorldView image to ensure the area represents homogeneous habitat even if spectral noise (e.g., canopy shading) was present in higher-resolution images. Final habitat classes included mangrove, saltmarsh, mudflat,

water, urban and upland vegetation. We randomly sampled 1000 pixels per class to create a balanced training dataset for each image. Data for each training sample included the observed habitat class and covariates derived from imagery bands and indices: blue, green, red, near-infrared (NIR), NDVI, NDWI, SR and GCVI.

Classification algorithm comparison

We tested the modeling accuracy of different supervised classification algorithms in performing landcover classifications in order to select the best algorithm to use for our set of images. Random Forest (Breiman, 2001), XGBoost (Friedman, 2001), K-nearest neighbor (Samworth, 2012) and neural network (Géron, 2022) algorithms were tested using the 'tidymodels' package in R (v1.0.0; Kuhn & Wickham, 2020). To assess model performance, we split the training dataset into a training set (75%) for fitting models and a testing set (25%) for evaluating model accuracy. The validation set used a 10-fold cross-validation and stratified sampling among classes. We tuned and evaluated model performance using the cross-validation set and selected the best algorithm based on model accuracy, Cohen's kappa coefficient, F score and ROC area under the curve (AUC) (Table S2).

Landcover classification

The selected algorithm for each image was tuned a final time to create a final classification model with the optimal model parameter values to maximize model performance. Final models were then applied to the full image across our study area in order to predict land cover classes based on the pixel values of all covariate bands and indices. Random Forest was ultimately selected as the final classification algorithm used for all images, as it performed better or was similar to other algorithms (Table S1) and is commonly used and successful in landcover applications (Talukdar et al., 2020).

Classification outputs included landcover maps of predicted mangrove, saltmarsh, mudflat, water, urban/built and upland vegetation habitats. Landcover map outputs were produced for each image in their native resolution. We cleaned landcover predictions using a majority filter to remove speckling (interclass noise) for areas connected by 4 or less pixels, opting for pixel counts over area to deal with large differences in pixel sizes. We performed an additional cleaning step using a weighted filter to remove mangrove and saltmarsh areas of connected pixels that were completely contained in urban/built and upland vegetation classes, as these represent potential misclassifications due to confusion among specific classes (Table S3). For our final maps, accuracy assessment and landscape metrics analysis, we focused on the mangrove and saltmarsh classes by reclassifying and combining water, bare soil, urban and upland vegetation classes to an 'other' class.

Landcover accuracy assessment and area estimation

We assessed the accuracy of the predicted landcover maps using a stratified random sample among mangroves, saltmarsh and other class pixels at 30 m resolution. Sample sizes per class were weighted by the average proportion of area of each class in the predicted landcover maps for a total of 450 samples. For each sample, we compared the actual habitat observed in WorldView and Google Basemaps for 2022 to the habitat predicted in each image. From this independent validation dataset, we calculated area-based error matrices following Olofsson et al. (2014), which allowed us to quantify the standard error and confidence intervals for the estimated area of each habitat, as well as user's, producer's accuracy and overall classification accuracy and kappa coefficients.

We compared the area estimates of mangrove and saltmarsh from the resulting classification maps to regional and global landcover datasets. We used the Florida Department of Environmental Protection 2017 Statewide Land Use and Land Cover (LULC) dataset to summarize the total area of mangroves and saltmarshes previously delineated within the study area (FL DEP, 2017). We also compare the amount of area within the study site included in global maps of mangroves (Giri et al., 2011; Bunting et al., 2022), saltmarsh (McOwen et al., 2017) and intertidal habitats that represent tidal marsh, tidal flat or mangrove ecosystems (Murray et al., 2019).

Landscape, class and patch metrics for mangrove and saltmarshes

We calculated landscape metrics from our classification maps to compare how image resolution impacted our ability to measure landscape composition and complexity, class dominance and spatial properties of habitat patches using the 'landscapemetrics' package in R (v2.0.0; Hesselbarth et al., 2019), which implements 'FRAGSTATS' analyses for landscape spatial patterns (McGarigal & Marks, 1995). At the landscape level, we quantified overall habitat configuration using the landscape shape index (LSI), which is the ratio between the total edge length of habitats and the minimum possible edge length defined by 1 pixel (Patton, 1975). Higher LSI values indicate increasingly complex, less compact habitat boundaries on the landscape. Overall landscape complexity was estimated using marginal entropy as the measure of diversity among

thematic landscape classes, where more dispersed, complex patterns have higher entropy (Nowosad & Stepinski, 2019). Landscape composition was summarized as the fractional cover of mangrove and saltmarsh habitats within a 1-km hex grid over the study area, which we displayed using a bivariate legend with three natural (Jenks) breaks from the 'biscale' R package (v1.1.0.9; Prener et al., 2022).

At the class level, we estimated the total number of patches and patch density per square kilometer for the mangrove and saltmarsh classes from each image. Class configuration on the landscape was summarized using the clumpiness index and the patch cohesion index. Class clumpiness indices indicate more random (0) or aggregated (1) distributions of classes based on the deviation of the proportion of same-class adjacencies compared to a spatially random distribution with the corresponding class (McGarigal & Marks, 1995). Patch cohesion indices estimate how connected or isolated patches of the same class are across the landscape (Schumaker, 1996). We estimated the mean fractal dimension index (FDI), which is a scale-dependent shape index based on patch perimeter and area that describes patch complexity (Mandelbrot, 1977). It has been suggested that FDI may indicate scaling factors to correct for the variability lost in habitat edges at coarser increasing resolutions, but more work is needed (Turner & Gardner, 2015), so we tested this among our classification outputs.

Patch-level metrics were used to summarize mean patch size, shape and connectedness detected for each class in each image. In addition to mean area, we also calculated the core area index, which equals the percentage of interior (non-edge pixels) area relative to total patch area. Patch complexity was estimated using the perimeter–area ratio. Patch intra-connectedness was summarized using the contiguity index, a shape metric representing the spatial contiguity of pixels within a patch (LaGro, 1991). Patch interconnectedness, or isolation, was estimated as the Euclidean nearest-neighbor (ENN) distance, which measures the edge-to-edge distance to the nearest patch of the same class (McGarigal & McComb, 1995).

Results

Mangrove classification using random forest improves with image resolution

VHR WorldView had the highest overall accuracy (84.2%) in classifying mangrove, saltmarsh and other habitats using Random Forest compared to Planet (82.2%), Sentinel (81.4%) and Landsat (50.6%) (Table 1). We found that Random Forest was the best overall supervised classification approach compared to other machine learning algorithms to use on each image (Table S2). The overall accuracy of the resulting landcover maps decreased as image resolution decreased. WorldView, Planet and Sentinel imagery performed similarly in terms of overall accuracy (81.4–84.2%) and kappa value (0.67–0.72), while 30-m Landsat showed a large decrease in accuracy (50.6%, 0 kappa value) using this classification approach.

Mangrove habitats were more often correctly identified as mangrove in the WorldView imagery (67% user's accuracy), compared to 46% in Planet, 38% in Sentinel and 13% in Landsat (Table 1). Mangroves were most often misclassified as 'other', namely upland vegetation (Table S3). Producer's accuracy of the mangrove class ranged from 60% to 73% across the images, showing a slight advantage in WorldView's ability to correctly identify 5% more of the mangrove reference training data. The landcover predictions at the leading edge of the range limit display the increased edge definition and detection of small patches of mangroves adjacent to tidal creeks with WorldView (Fig. 2).

Saltmarsh habitats were classified correctly 76% of the time using WorldView, 82% using Planet and 72% using Sentinel (Table 1). Landsat did not predict any saltmarsh in our classification approach, explaining why the user's accuracy for this class is 0% and overall kappa is 0. Aside

TABLE 1. Landcover accuracy and corrected area estimates (±95% CI) of Random Forest classification maps. Overall accuracy and Kappa values per image summarize users' and producers' accuracy among mangrove, saltmarsh and other classes.

	WorldView				Planet				Sentinel				Landsat			
Overall accuracy	84.2				82.2				81.4				50.6			
Kappa value	0.72				0.68				0.67				0			
Class	UA (%)	PA (%)	Area (ha)	95% CI (ha)	UA (%)	PA (%)	Area (ha)	95% CI (ha)	UA (%)	PA (%)	Area (ha)	95% CI (ha)	UA (%)	PA (%)	Area (ha)	95% CI (ha)
Mangrove	67	73	800.0	214.4	46	60	590.8	215.1	38	68	373.3	169.6	13	68	125.6	107.7
Saltmarsh	76	94	3234.9	281.3	82	88	4961.0	377.2	72	93	3385.8	319.2	0	NA	NA	NA
Other	94	80	5953.9	335.1	88	80	6100.9	403.8	95	76	6308.8	338.6	99	50	9942.3	107.7

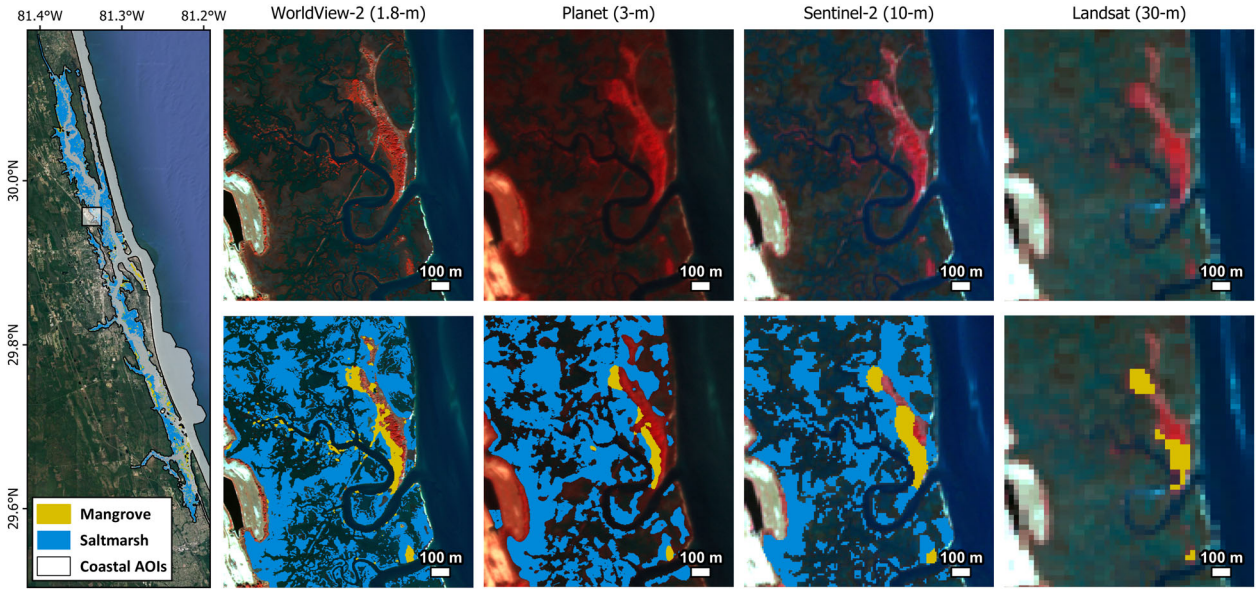

Figure 2. Comparison of false-color images per satellite and landcover maps of mangrove individuals and stands (yellow) and saltmarshes (blue) at the northern edge of the mangrove range limit in Florida, USA. WorldView Basemaps © 2022 Maxar/DigitalGlobe, Inc. Basemap © 2022 ESRI.

from Landsat, the saltmarsh class was more accurate to map (88–94% producer's accuracy) compared to the mangrove class (60–73%). Saltmarsh was most often misclassified with mudflat at moderate resolutions and mangrove and upland vegetation at higher resolutions (Table S3). A large saltmarsh patch in the south of our study area identified with WorldView, Planet and Sentinel highlights where image resolution and class confusion impact the delineation of saltmarsh edges (Fig. 3).

VHR imagery detects more mangroves compared to moderate imagery and regional and global maps

The total area of mangroves detected in our study region using WorldView was estimated at 800.0 ± 214.4 ha (Table 1, Fig. 4A). That is 35% more mangrove area than was classified with Planet (590.8 ± 215.1 ha), 114% more than Sentinel (373.3 ± 169.6 ha) and 537% more than

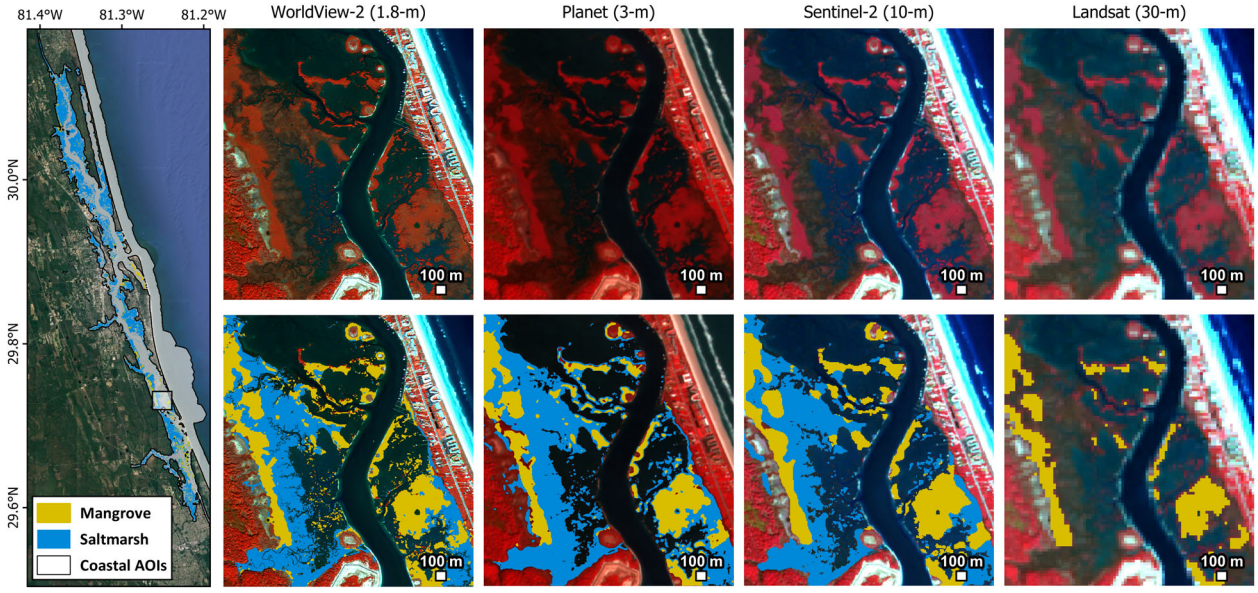

Figure 3. Comparison of false-color images per satellite and landcover maps of mangroves (yellow) and saltmarshes (blue) in the southern portion of the mangrove range limit in Florida, USA. WorldView Basemaps © 2022 Maxar/DigitalGlobe, Inc. Basemap © 2022 Google.

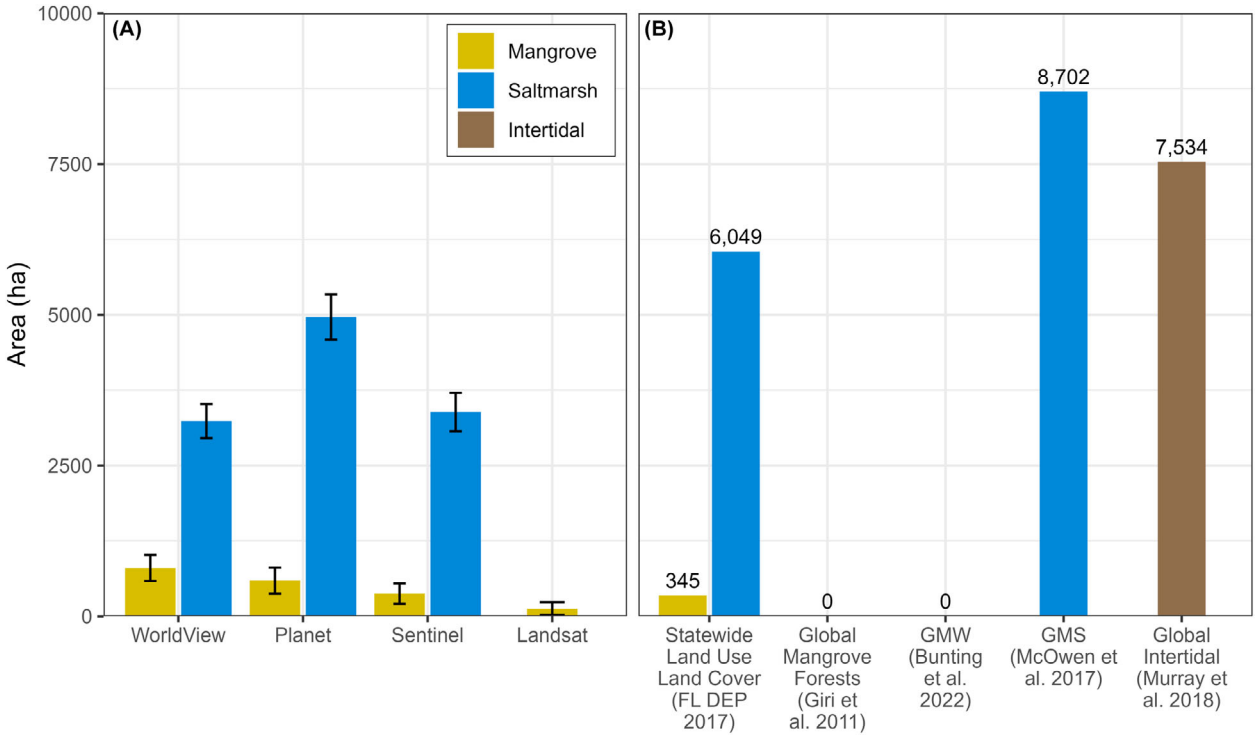

Figure 4. Mangrove and saltmarsh areas classified in (A) this study compared to (B) regional and global coastal datasets within the study region.

Landsat (125.6 ± 107.7 ha). Planet predicted the most saltmarsh area (4961.0 ± 377.2 ha), followed by 3385.8 ± 319.2 ha predicted with Sentinel, 3234.9 ± 281.3 ha predicted with WorldView and 0 ha predicted with Landsat (Table 1). Despite similar accuracies among WorldView, Planet and Sentinel classifications (81.4–84.2%), they estimated substantially different proportions of mangrove and saltmarsh across the landscape (Fig. 5). Total mangrove area estimates ranged from 125.6 to 800.0 ha across all images, while the estimated range of saltmarsh area varied from 0.0 to 4961.0 ha (Table 1, Fig. 4A). The mangrove class was most accurately mapped with WorldView (67% user's accuracy) which estimated the most mangroves (800.0 ± 214.4 ha). Similarly, the most saltmarsh (4961.0 ± 377.2 ha) was predicted with Planet, which also had the highest user's accuracy (82%).

The 800.0 ha of mangroves we identified represent an additional 455.0 ha of mangroves that were not included in the 345.0 ha of mangroves mapped in the 2017 FL statewide landcover dataset (Fig. 4B). For saltmarshes, our classifications underestimated the 6,049 ha mapped by FL DEP by −47% using WorldView, −44% using Sentinel and −100% using Landsat, but just −17% with Planet. Compared to global maps, our classifications detected upwards of 800.0 ha of mangroves that were not identified in the 2011 Global Mangrove Forest or 2022 Global Mangrove Watch datasets (Giri et al., 2011; Bunting et al., 2022). However, compared to the 8,702 ha of saltmarsh in our study area (2017 Global Map of Saltmarsh; McOwen et al., 2017) and to the 7534 ha of intertidal (2018 Global Intertidal Map; Murray et al., 2019), overall, our classifications underestimated both the total saltmarsh area and the combined wetland area (saltmarsh and mangrove) by as much as 93% and 26%, respectively (Fig. 4).

Complexity of mangrove and saltmarsh habitats at range limits increases with image resolution

At the landscape level, the proportion of mangrove and saltmarsh habitats derived from the multiresolution classifications largely revealed similar distributions throughout the range limit and identified large habitat patches (Figs. 5 and 6A). Mangroves dominated coastal areas (<40%) south of 29.9°N in all images. Saltmarshes occupied a higher proportion of coastal area (<80%) largely to the north and in several large patches to the south (Fig. 5). The complexity of habitats, measured as LSI, decreased as image resolution increased, with WorldView (LSI = 158.4) identifying 1067% more complexity in

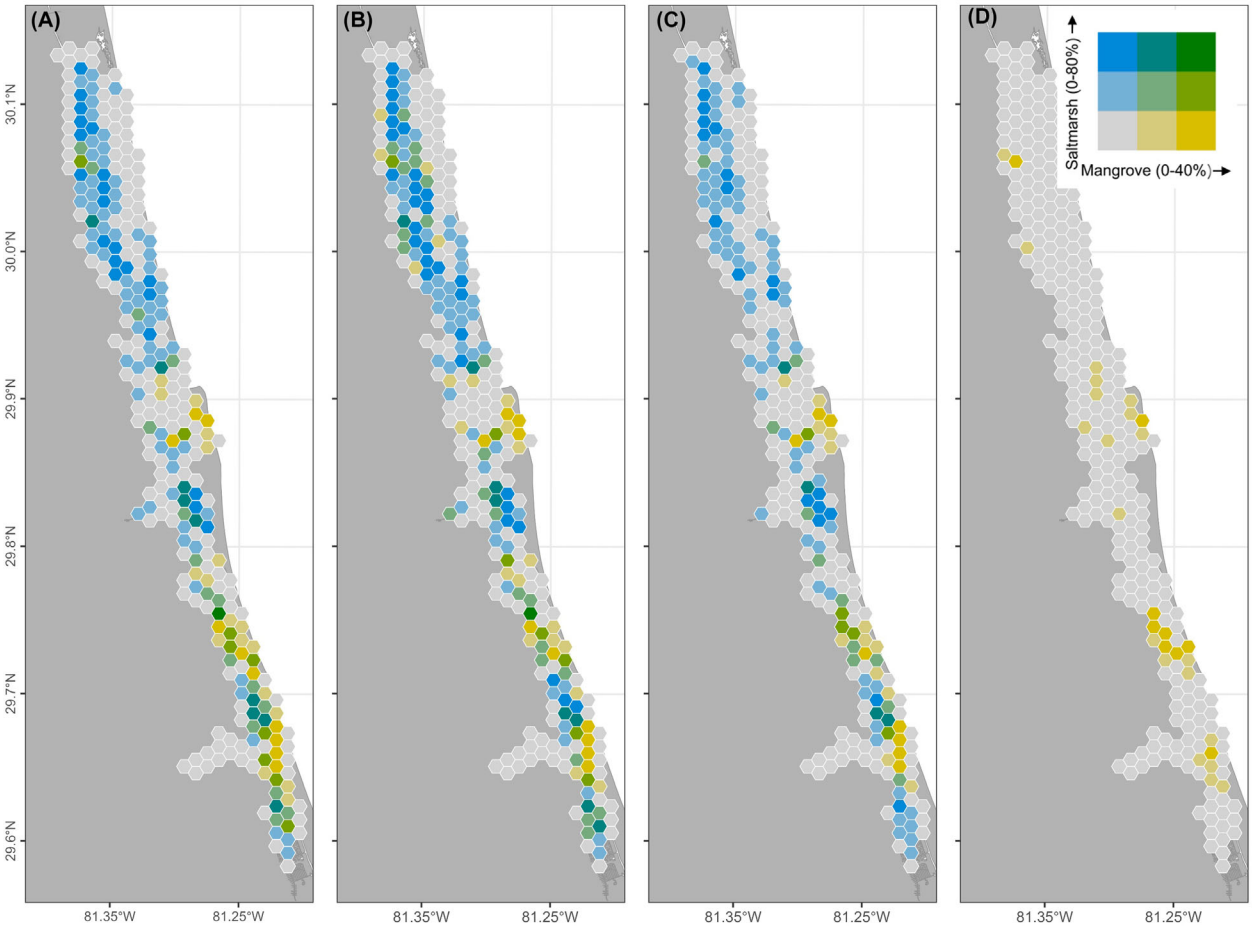

Figure 5. Landscape composition of mangrove (yellow) and saltmarsh (blue) habitats proportionate cover detected with (A) WorldView, (B) Planet, (C) Sentinel and (D) Landsat.

habitat edges than Landsat (LSI = 13.7, Fig. 6A). Planet and Sentinel LSI estimates were 79.6 and 64.1, respectively, indicating similar measures of habitat configuration detected at 3-m and 10-m image resolutions. Marginal entropy, the metric for thematic complexity, was highest for WorldView (0.64), followed by Sentinel (0.55) and Planet (0.46).

At the class level (Fig. 6B), patch counts and density for the mangrove class were highest in WorldView with 5848 patches at 123.2 patches km^{-2}, more than the 1142 patches from Planet (19.6 patches km^{-2}), the 457 from Sentinel (9.2 patches km^{-2}) and 142 patches from Landsat (55.1 patches km^{-2}). Similarly, counts of saltmarsh patches identified were highest in WorldView (13 899), more than the 5665 patches from Planet, the 2750 patches from Sentinel and no patches identified from Landsat (Fig. 6B, Table S4). Patch clumpiness indices for both mangrove and saltmarsh fell within a small range from 0.971 to 0.977 for WorldView, Planet and Sentinel images, which indicates similar detection of highly uneven spatial aggregation among the two classes across the landscape. Patch cohesion indices measuring intraclass connectedness of mangroves increased with image resolution: WorldView (98.6), Planet (98.3), Sentinel (96.1) and Landsat (89.5). No pattern appeared with image resolution in the cohesion indices for saltmarsh, which suggests that increased image resolutions help detect more connections only for the highly aggregated mangrove class. FDI, a metric of patch complexity, increased with image resolution for both classes. Mangrove FDI was 1.120 ± 0.077, 1.103 ± 0.059, 1.075 ± 0.050 and 1.045 ± 0.041 for Worldview, Planet, Sentinel and Landsat, respectively. Saltmarsh FDI was 1.121 ± 0.090, 1.076 ± 0.073 and 1.066 ± 0.061, for Worldview, Planet and Sentinel, respectively.

At the patch level, image resolution impacted landscape metrics describing patch size, shape and connectedness per class (Fig. 6C). Mean mangrove patch areas were

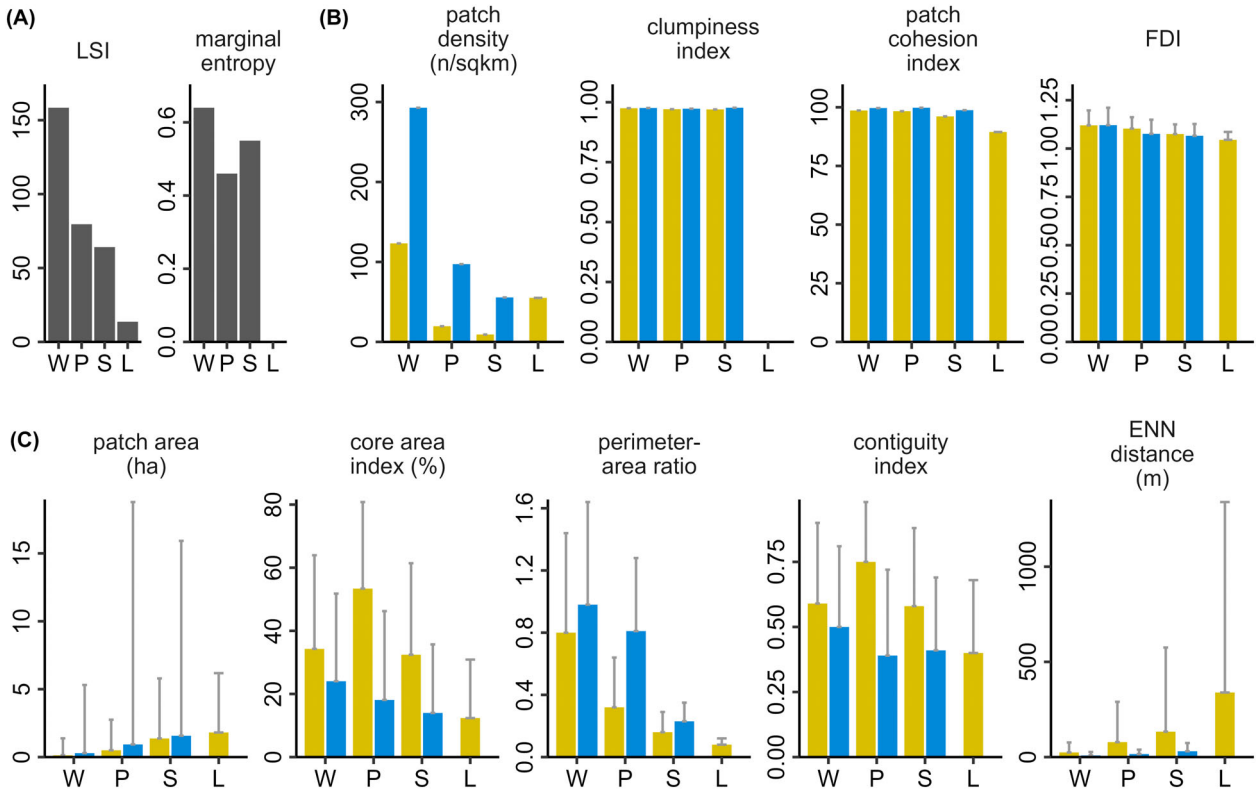

Figure 6. Landcover metrics at the (A) landscape, (B) class and (C) patch levels for mangrove (yellow) and saltmarsh (blue) detected from WorldView (W), Planet (P), Sentinel (S) and Landsat (L). Values reported for classes and patches are means ± standard (see Table S4). Note that only the mangrove class was present for Landsat.

0.13 ± 1.25 ha for WorldView, 0.50 ± 2.25 ha for Planet, 1.37 ± 4.42 ha for Sentinel and 1.81 ± 4.37 ha for Landsat. Mean saltmarsh patch areas were 0.29 ± 5.02 ha for WorldView, 0.93 ± 17.85 ha for Planet and 1.57 ± 14.35 ha for Sentinel. The mean core area index varied greatly among classes and imagery with higher values in the mangrove class indicating more compact, or square, patch shapes compared to the relatively more complex shapes of saltmarsh habitats detected in the same image. Core area index for Planet-derived mangroves was 53.4 ± 27.4%, while WorldView and Sentinel produced more similar estimates of 34.3 ± 29.7% and 32.4 ± 28.9%, respectively. Perimeter–area ratios per class increased with resolution, as the complexity in patch boundaries is increasingly revealed with higher-resolution imagery (Fig. 6C; Table S4).

The contiguity index measuring patch interconnectivity was 18% higher on average in mangroves (0.59 ± 0.31) versus saltmarsh (0.50 ± 0.31) from WorldView, nearly doubled in mangroves (0.75 ± 0.23) versus saltmarsh (0.39 ± 0.33) from Planet and 42% higher on average in mangroves (0.58 ± 0.30) versus saltmarsh (0.41 ± 0.28) from Sentinel. Landsat mangrove contiguity was an estimated 0.40 ± 0.28. Higher contiguity index values indicate more contiguous patches. ENN distance measuring the connection among same-class patches decreased with image resolution for the mangrove class, but not the saltmarsh class. The mean distance detected between mangrove patches was 24.4 ± 52.2 m in WorldView, 78.5 ± 211.7 m in Planet, 133.5 ± 441.7 m in Sentinel and 339.1 ± 1000.4 m in Landsat. ENN distances were smaller for saltmarsh patches overall compared to mangrove: WorldView (8.6 ± 18.2 m), Planet (15.7 ± 23.0 m), Sentinel (30.7 ± 43.2 m) and none in Landsat.

Discussion

Discrepancies between the scales of mangrove observation and mapping have led to uncertainty in the limits and extents of mangroves at the leading edge of their geographical ranges, but we found by comparing across different satellite images that mapping at higher resolutions can supplement regional and global mapping efforts and reveal important ecological properties at local scales. Along the northeast Florida coastline, VHR mapping

uncovered at least 240.6 ha of mangroves that were previously unmapped. These vanguard mangroves represent the leading edge of this range shift and are important to monitor as encroaching mangroves influence ecosystem services and future responses to climate change.

Mapping at higher resolutions is necessary to supplement our global understanding of mangrove distributions and dynamics. In some range limits across the world, especially in western North America, western Australia and northern West Africa, latitudinal discrepancies of up to 10° exist in the detected limits from each global dataset, and this has significant consequences as we make global inferences on the climatic drivers of mangrove change or make area-based extrapolations of global mangrove carbon accounting, deforestation rates and mitigation potential (Ximenes et al., 2022). Our mapping analysis across different scales estimated different total extents of mangrove and saltmarsh habitats, however, all sensors were able to detect the same large northward patch of mangroves within our study area at 29.959471°N, 81.330311°W. This same patch was the northernmost mangrove mapped in the FL LCLUC (2017) but was missing from global maps. The patch extent derived from only partial coverage with Landsat was 1.32 ha, whereas Sentinel, Planet and WorldView identified the patch size as 2.31, 1.77 and 2.97 ha, respectively. Compared to this patch, the northernmost patch of mangroves identified by Sentinel was located c. 6.2 km to the north (30.0141906°N, 81.3446904°W). With Planet, the northernmost patch detected was just 442 m to the north (29.9632769°N, 81.3318483°W). Worldview identified the northernmost patch of mangroves 11.65 km further than Landsat (30.05996325°N, 81.36519184°W). The northernmost patches detected in all images were within 0.1° latitude.

Comparing mangrove extents derived from different methodological approaches or points in time makes it challenging to assess change within the mangrove–saltmarsh ecotone. We estimated a total of 800.0 ± 214.4 ha of mangroves as of 2022 using WorldView. The best available estimate of 345 ha of mangroves in the region from the FL DEP LULC dataset was published in 2017 and is based on earlier data dating back to 2012 (FL DEP, 2017). The updated FL Cooperative Land Cover Map (FL Fish and Wildlife Conservation Commission, 2022) is based on data from 2018 to 2021, however, some mangroves in the study area are now reclassified as other coastal habitats. Although we cannot interpret the difference as true mangrove gains or losses from 2017 to 2023, we estimated less saltmarsh in all three of our higher-resolution classifications compared to the 6049 ha of saltmarsh mapped in the FL DEP LULC dataset and 8702 ha identified in the Global Map of Saltmarsh dataset (McOwen et al., 2017). Marsh loss has been predicted in areas of the GTMNERR using field-based measures of saltmarsh productivity to parameterize a tide–marsh equilibrium model, Hydro-MEM (Bacopoulos et al., 2019). The coastal wetland equilibrium model (CWEM), developed specifically to predict future response to sea level rise (SLR) in mangrove-saltmarsh ecotones, also found that although mangroves have higher surface elevation gain rates than saltmarsh, the elevation gain is abruptly lost with mangrove mortality and both habitat types are projected to drown under SLR of 100 cm (Morris et al., 2023). SLR-induced changes will not be limited to saltmarshes, as the landward migration of mangroves is expected to displace adjacent freshwater and upland ecosystems (Osland, Chivoiu, et al., 2022). In addition to SLR, boat wakes and coastal storms will add to the vulnerability of the mangrove–saltmarsh ecotone (Verutes et al., 2024). Improved maps of current mangrove distribution at range limits will allow us to more directly assess coastal wetlands changes, gains and losses at relevant scales.

Our approach to range-limit mapping identified important spatial patterns across the mangrove–saltmarsh ecotone that will likely have consequences to ecosystem structure, function and services as the landscape continues to undergo rapid climate-driven changes. Understanding the boundaries of habitats at range limits is necessary to understand mangrove dispersal and connect establishment dynamics across plot, patch and landscape scales (Yando et al., 2021). WorldView, Planet and Sentinel images indicated similar patterns of highly uneven spatial aggregation among the two classes across the landscape, but high resolutions provided more insights into patch inter- and intra-class connectivity measured by contiguity indices and ENN distances. The spatial relationship between mangroves and saltmarsh measured by satellites is the culmination of ecological phenomena occurring at fine scales. Eutrophication has been attributed to mangrove expansion in the region, as nitrogen availability increases mangrove growth, canopy size and reproduction (Dangremond et al., 2020). Mangroves pioneering the leading edge have shown precocious reproductive rates and adaptive genetic traits, which can accelerate population growth and expansion into salt marsh (Dangremond & Feller, 2016; Kennedy et al., 2022). Recruitment of mangrove propagules into adjacent habitats can also be influenced by grass or succulent saltmarsh growth forms and by spring or storm tidal events (Peterson & Bell, 2012, 2015; Adgie & Chapman, 2021). Boundaries created by tides and saltmarsh properties ultimately influence where propagules can disperse and recruit, resulting in different landward versus seaward expansion (Peterson & Bell, 2015). Abiotic conditions at fine scales, namely

temperature, precipitation, hydrology and salinity, can also impact growth rates, belowground biomass allocation and carbon storage of each habitat differently in addition to dispersal in changing saltmarsh and mangrove ecotones (Yando et al., 2016, 2018, 2021; Chapman et al., 2021).

The spatial relationships we found among landscape metrics in mangrove and saltmarsh habitats in northeastern Florida at multiple resolutions could potentially provide a basis for quantifying uncertainty in mangrove extents or for correcting for differences in area detected among satellite sensors. The fractal dimension index (FDI) summarizes the complexity of patch edges, with the underlying assumption that smaller units of measurement allow us to measure more variation in the habitat perimeter. Coastlines typically have fractal dimensions around 1.2 (Lam & Quattrochi, 1992). We found FDI for mangrove patches unsurprisingly increased with image resolution, from 1.045 ± 0.041 with Landsat to 1.120 ± 0.077 with WorldView. Using the WoldView FDI as a scaling factor to correct Landsat estimates, we would estimate that the 125.6 ± 107.7 ha of mangrove measured by Landsat in this study could really represent upward of 277.7 ha of mangroves if the same areas were measured at the scale of 1.8 m versus 30 m. Sentinel and Planet estimates could similarly be revised upward to 646.1 and 958.0 ha, respectively. However, more work needs to be done to test using FDI as a scaling factor in different mangrove regions before being used to bookend uncertainty in mangrove area estimates.

Multiresolution classification highlights the tradeoffs between the spatial resolution of satellite imagery, the global coverage of satellite data and the computational power required to run machine learning models. At local to regional scales, fine-scale mapping efforts can require extensive time and resources for manual digitization. We observed that 1.8-m WorldView and 10-m Sentinel performed similarly in correctly classifying mangrove and saltmarsh areas and in identifying similar patterns in class clumpiness, cohesion and shape/compactness on the landscape, despite differences in overall estimated extents. Landscape metrics of habitat complexity, patch density, patch complexity, patch size, edge complexity and connectedness per class, however, were found to improve with image resolutions. In addition to the resolution of satellite imagery, data accessibility and the ease of working with public versus commercial satellite data on large geographic scales will be important tradeoffs to consider in selecting the correct data to measure ecological phenomena at range limits.

No matter how fine the scales are at which we conduct remote sensing, our ability to detect mangrove expansion at the leading edge will always be limited, but the scales at which analyses are conducted and observations are made matter (Li and Wu 2004). Our work illustrates that VHR improves mapping and identification of landscape, class and patch properties of mangroves and saltmarshes at the leading edge of a range limit. We identified the northernmost mangrove patch within our study area at 30.05996325°N, 81.36519184°W with remote sensing, which is still 0.4° south of the northernmost reported field observation of mangroves made in the Timucuan Ecological and Historic Preserve near Jacksonville, Florida, in recent years (Cavanaugh et al., 2019). These pioneer mangroves have since suffered diebacks caused by extreme freeze events (Kaalstad et al. 2023), further emphasizing the need for more dynamic mapping approaches. The scales of the satellite imagery tested in this study are not capable of detecting individual seedlings; however, unoccupied aerial systems (UASs) that can collect imagery at centimeter scales may provide more appropriate scales for observation. As higher and higher resolutions become available, it may become easier to identify mangroves newly emerging into saltmarsh and other coastal habitats. There is a clear need for better coordinated regional networks of coastal monitoring that use consistent very high resolution spatiotemporal data and methods paired with field observations to advance the understanding of past, current and future coastal dynamics in the southeastern United States and beyond (Bardou et al. 2023). For the time being, no remote sensing can replace the power of fieldwork in uncovering mangrove pioneers at the leading edge, and more work will be needed to further reduce the gap between our field and remotely sensed observations.

Acknowledgments

Cheryl Doughty's research was supported by an appointment to the National Aeronautics and Space Administration (NASA) Postdoctoral Program at the NASA Goddard Space Flight Center, administered by the Oak Ridge Associated Universities under contract with NASA. This research was also supported by the National Aeronautics and Space Administration (NASA) Land Use/Land Cover Change Program (grant number WBS437949.02.06.01.36).

Conflict of Interest Statement

The authors declare no conflict of interest.

References

Adame, M.F., Connolly, R.M., Turschwell, M.P., Lovelock, C.E., Fatoyinbo, T., Lagomasino, D. et al. (2021) Future carbon emissions from global mangrove forest loss. *Global Change Biology*, **27**, 2856–2866.

Adgie, T.E. & Chapman, S.K. (2021) Salt marsh plant community structure influences success of *Avicennia germinans* during poleward encroachment. *Wetlands*, **41**, 82.

Bacopoulos, P., Tritinger, A.S. & Dix, N.G. (2019) Sea-level rise impact on salt marsh sustainability and migration for a subtropical estuary: GTMNERR (Guana Tolomato Matanzas National Estuarine Research Reserve). *Environmental Modeling & Assessment*, **24**, 163–184.

Bardou, R., Osland, M.J., Scyphers, S., Shepard, C., Aerni, K.E., Alemu, J.B. et al. (2023) Rapidly changing range limits in a warming world: critical data limitations and knowledge gaps for advancing understanding of mangrove range dynamics in the Southeastern USA. *Estuaries and Coasts*, **46**, 1123–1140.

Breiman, L. (2001) Random forests. *Machine Learning*, **45**, 5–32.

Bryan-Brown, D.N., Connolly, R.M., Richards, D.R., Adame, F., Friess, D.A. & Brown, C.J. (2020) Global trends in mangrove forest fragmentation. *Scientific Reports*, **10**, 7117.

Bunting, P., Rosenqvist, A., Hilarides, L., Lucas, R.M. & Thomas, N. (2022) Global mangrove watch: updated 2010 mangrove Forest extent (v2.5). *Remote Sensing*, **14**, 1034.

Bunting, P., Rosenqvist, A., Lucas, R.M., Rebelo, L.M., Hilarides, L., Thomas, N. et al. (2018) The global mangrove watch – a new 2010 global baseline of mangrove extent. *Remote Sensing*, **10**, 1669.

Campbell, A.D., Fatoyinbo, L., Goldberg, L. & Lagomasino, D. (2022) Global hotspots of salt marsh change and carbon emissions. *Nature*, **612**, 701–706.

Cavanaugh, K.C., Dangremond, E.M., Doughty, C.L., Williams, A.P., Parker, J.D., Hayes, M.A. et al. (2019) Climate-driven regime shifts in a mangrove-salt marsh ecotone over the past 250 years. *Proceedings of the National Academy of Sciences of the United States of America*, **116**(43), 21602–21608. Available from: https://doi.org/10.1073/pnas.1902181116

Cavanaugh, K.C., Kellner, J.R., Forde, A.J., Gruner, D.S., Parker, J.D., Rodriguez, W. et al. (2014) Poleward expansion of mangroves is a threshold response to decreased frequency of extreme cold events. *Proceedings of the National Academy of Sciences of the United States of America*, **111**, 723–727.

Cavanaugh, K.C., Osland, M.J., Bardou, R., Hinojosa-Arango, G., López-Vivas, J.M., Parker, J.D. et al. (2018) Sensitivity of mangrove range limits to climate variability. *Global Ecology and Biogeography*, **27**, 925–935.

Chapman, S.K., Feller, I.C., Canas, G., Hayes, M.A., Dix, N., Hester, M. et al. (2021) Mangrove growth response to experimental warming is greatest near the range limit in northeast Florida. *Ecology*, **102**, e03320.

Coldren, G.A., Langley, J.A., Feller, I.C. & Chapman, S.K. (2019) Warming accelerates mangrove expansion and surface elevation gain in a subtropical wetland. *Journal of Ecology*, **107**, 79–90.

Dangremond, E.M. & Feller, I.C. (2016) Precocious reproduction increases at the leading edge of a mangrove range expansion. *Ecology and Evolution*, **6**, 5087–5092.

Dangremond, E.M., Simpson, L.T., Osborne, T.Z. & Feller, I.C. (2020) Nitrogen enrichment accelerates mangrove range expansion in the temperate–tropical ecotone. *Ecosystems*, **23**, 703–714.

Davidson, N.C., Fluet-Chouinard, E., Finlayson, C.M., Davidson, N.C., Fluet-Chouinard, E. & Finlayson, C.M. (2018) Global extent and distribution of wetlands: trends and issues. *Marine and Freshwater Research*, **69**, 620–627.

Dix, N.G., Brockmeyer, R., Chapman, S.K., Angelini, C., Kidd, S., Eastman, S.F. et al. (2021) Northest Florida. In: Radabaugh, K.R., Powell, C.E. & Moyer, R.P. (Eds.) *Coastal habitat integrated mapping and monitoring program report for the state of Florida*. St. Petersburg, FL: Florida Fish and Wildlife Conservation Commission Fish and Wildlife Research Institute Technical Report No. 21, version 2..

Doughty, C. & Cavanaugh, K. (2019) Mapping coastal wetland biomass from high resolution unmanned aerial vehicle (UAV) imagery. *Remote Sensing*, **11**, 540.

Doughty, C.L., Ambrose, R.F., Okin, G.S. & Cavanaugh, K.C. (2021) Characterizing spatial variability in coastal wetland biomass across multiple scales using UAV and satellite imagery. *Remote Sensing in Ecology and Conservation*, **7**, 411–429.

Doughty, C.L., Cavanaugh, K.C., Hall, C.R., Feller, I.C. & Chapman, S.K. (2017) Impacts of mangrove encroachment and mosquito impoundment management on coastal protection services. *Hydrobiologia*, **803**, 105–120.

Doughty, C.L., Langley, J.A., Walker, W.S., Feller, I.C., Schaub, R. & Chapman, S.K. (2016) Mangrove range expansion rapidly increases coastal wetland carbon storage. *Estuaries and Coasts*, **39**, 385–396.

FL Department of Environmental Protection (DEP). (2017) Statewide Land Use Land Cover.

FL Fish and Wildlife Conservation Commission (FWC). (2022) Cooperative Land Cover Map.

Foody, G.M. (2023) Remote sensing in landscape ecology. *Landscape Ecology*, **38**, 2711–2716.

Friedman, J.H. (2001) Greedy function approximation: a gradient boosting machine. *The Annals of Statistics*, **29**, 1189–1232.

Geoghegan, E.K., Langley, J.A. & Chapman, S.K. (2021) A comparison of mangrove and marsh influences on soil respiration rates: a mesocosm study. *Estuarine, Coastal and Shelf Science*, **248**, 106877.

Géron, A. (2022) Hands-on machine learning with scikit-learn, keras, and tensorflow.

Giri, C., Ochieng, E., Tieszen, L.L., Zhu, Z., Singh, A., Loveland, T. et al. (2011) Status and distribution of mangrove forests of the world using earth observation satellite data. *Global Ecology and Biogeography*, **20**, 154–159.

Goeke, J.A., Foster, E.M. & Armitage, A.R. (2023) Negative outcomes of novel trophic interactions along mangrove range edges. *Ecology*, **104**, e4051.

Goldberg, L., Lagomasino, D., Thomas, N. & Fatoyinbo, T. (2020) Global declines in human-driven mangrove loss. *Global Change Biology*, **26**, 5844–5855.

Gorelick, N., Hancher, M., Dixon, M., Ilyushchenko, S., Thau, D. & Moore, R. (2017) Google earth engine: planetary-scale geospatial analysis for everyone. *Remote Sensing of Environment*, **202**, 18–27.

Grizonnet, M., Michel, J., Poughon, V., Inglada, J., Savinaud, M. & Cresson, R. (2017) Orfeo ToolBox: open source processing of remote sensing images. *Open Geospatial Data, Software and Standards*, **2**, 15.

Hamilton, S.E. & Casey, D. (2016) Creation of a high spatio-temporal resolution global database of continuous mangrove forest cover for the 21st century (CGMFC-21). *Global Ecology and Biogeography*, **25**, 729–738.

Hansen, M.C., Potapov, P.V., Moore, R., Hancher, M., a Turubanova, S., Tyukavina, A. et al. (2013) High-resolution global maps of 21st-century Forest cover change. *Science (New York, N.Y.)*, **850**, 2011–2014.

Hesselbarth, M.H., Sciaini, M., With, K.A., Wiegand, K. & Nowosad, J. (2019) Landscapemetrics: an open-source R tool to calculate landscape metrics. *Ecography*, **42**, 1648–1657.

Hickey, S.M. & Radford, B. (2022) Turning the tide on mapping marginal mangroves with multi-dimensional space–time remote sensing. *Remote Sensing*, **14**, 3365.

Howard, R.J., From, A.S., Krauss, K.W., Andres, K.D., Cormier, N., Allain, L. et al. (2020) Soil surface elevation dynamics in a mangrove-to-marsh ecotone characterized by vegetation shifts. *Hydrobiologia*, **847**, 1087–1106. Available from: https://doi.org/10.1007/s10750-019-04170-4

Kaalstad, S., Osland, M., Devlin, D., Proffitt, E., Feher, L., Armitage, A. et al. (2023) Temperature thresholds for leaf damage from two extreme freeze events (2018 and 2021) near the northern Range limit of black mangroves (*Avicennia germinans*) in southeastern North America. *Estuaries and Coasts*, **47**, 292–300. Available from: https://doi.org/10.1007/s12237-023-01279-7

Kamal, M., Hidayatullah, M.F., Mahyatar, P. & Ridha, S.M. (2022) Estimation of aboveground mangrove carbon stocks from WorldView-2 imagery based on generic and species-specific allometric equations. *Remote Sensing Applications: Society and Environment*, **26**, 100748.

Kamal, M., Phinn, S. & Johansen, K. (2014) Characterizing the spatial structure of Mangrove features for optimizing image-based mangrove mapping. *Remote Sensing*, **6**, 984–1006.

Kamal, M., Phinn, S. & Johansen, K. (2015) Object-based approach for multi-scale mangrove composition mapping using multi-resolution image datasets. *Remote Sensing*, **7**(4), 4753–4783.

Kelleway, J.J., Cavanaugh, K., Rogers, K., Feller, I.C., Ens, E., Doughty, C. et al. (2017) Review of the ecosystem service implications of mangrove encroachment into salt marshes. *Global Change Biology*, **23**, 3967–3983.

Kennedy, J.P., Johnson, G.N., Preziosi, R.F. & Rowntree, J.K. (2022) Genetically based adaptive trait shifts at an expanding mangrove range margin. *Hydrobiologia*, **849**, 1777–1794.

Klemas, V. (2011) Remote sensing techniques for studying coastal ecosystems: an overview. *Journal of Coastal Research*, **27**, 2–17.

Klemas, V. (2013) Airborne remote sensing of coastal features and processes: an overview. *Journal of Coastal Research*, **287**, 239–255.

Klemas, V.V. (2015) Coastal and environmental remote sensing from unmanned aerial vehicles: an overview. *Journal of Coastal Research*, **315**, 1260–1267.

Krause, J.R., Oczkowski, A.J. & Watson, E.B. (2023) Improved mapping of coastal salt marsh habitat change at Barnegat Bay (NJ, USA) using object-based image analysis of high-resolution aerial imagery. *Remote Sensing Applications: Society and Environment*, **29**, 1–11.

Kuhn, M. & Wickham, H. (2020) Tidymodels: a collection of packages for modeling and machine learning using tidyverse principles.

LaGro, J. (1991) Assessing patch shape in landscape mosaics. *Photogrammetric Engineering and Remote Sensing*, **57**, 285–293.

Lam, N.S.-N. & Quattrochi, D.A. (1992) On the issues of scale, resolution, and fractal analysis in the mapping sciences. *The Professional Geographer*, **44**, 88–98.

Lausch, A., Blaschke, T., Haase, D., Herzog, F., Syrbe, R.-U., Tischendorf, L. et al. (2015) Understanding and quantifying landscape structure – a review on relevant process characteristics, data models and landscape metrics. *Ecological Modelling*, **295**, 31–41.

Li, H. & Wu, J. (2004) Use and misuse of landscape indices. *Landscape Ecology*, **19**, 389–399.

Liu, A.J. & Cameron, G.N. (2001) Analysis of landscape patterns in coastal wetlands of Galveston Bay, Texas (USA). *Landscape Ecology*, **16**, 581–595.

López-Hoffman, L., Breshears, D.D., Allen, C.D. & Miller, M.L. (2013) Key landscape ecology metrics for assessing climate change adaptation options: rate of change and patchiness of impacts. *Ecosphere*, **4**, 1–18.

Lustig, A., Stouffer, D.B., Roigé, M. & Worner, S.P. (2015) Towards more predictable and consistent landscape metrics across spatial scales. *Ecological Indicators*, **57**, 11–21.

Mandelbrot, B.B. (1977) *Fractals: form, chance, and dimension*. San Francisco: W. H. Freeman and Company.

Maskey, M., A. Hall, K. Murphy, C. Tucker, W. McCarty, and A. Kaulfus. 2021. Commercial Smallsat Data Acquisition: Program Update. 600–603. 2021 IEEE International Geoscience and Remote Sensing Symposium IGARSS.

McCarthy, M.J., Merton, E.J. & Muller-Karger, F.E. (2015) Improved coastal wetland mapping using very-high 2-meter spatial resolution imagery. *International Journal of Applied Earth Observation and Geoinformation*, **40**, 11–18.

McFeeters, S.K. (1996) The use of the Normalized Difference Water Index (NDWI) in the delineation of open water features. *International Journal of Remote Sensing*, **17**, 1425–1432.

McGarigal, K. & Marks, B.J. (1995) *FRAGSTATS: spatial pattern analysis program for quantifying landscape structure*. Gen. Tech. Rep. PNW-GTR-351, Vol. **122**. Portland, OR: U.S. Department of Agriculture, Forest Service, Pacific Northwest Research Station, p. 351.

McGarigal, K. & McComb, W.C. (1995) Relationships between landscape structure and breeding birds in the Oregon coast Range. *Ecological Monographs*, **65**, 235–260.

McOwen, C.J., Weatherdon, L.V., Van Bochove, J.W., Sullivan, E., Blyth, S., Zockler, C. et al. (2017) A global map of saltmarshes. *Biodiversity Data Journal*, **5**, e11764.

Morris, J.T., Langley, J.A., Vervaeke, W.C., Dix, N., Feller, I.C., Marcum, P. et al. (2023) Mangrove Trees outperform saltmarsh grasses in building elevation but collapse rapidly under high rates of sea-level rise. *Earth's Future*, **11**(4). Available from: https://doi.org/10.1029/2022ef003202

Morrisey, D.J., Swales, A., Dittmann, S., Morrison, M.A., Lovelock, C.E. & Beard, C.M. (2010) The ecology and management of temperate mangroves. *Oceanography and Marine Biology: An Annual Review*, **48**, 43–160.

Murray, N.J., Phinn, S.R., DeWitt, M., Ferrari, R., Johnston, R., Lyons, M.B. et al. (2019) The global distribution and trajectory of tidal flats. *Nature*, **565**, 222–225.

Murray, N.J., Worthington, T.A., Bunting, P., Duce, S., Hagger, V., Lovelock, C.E. et al. (2022) High-resolution mapping of losses and gains of Earth's tidal wetlands. *Science*, **376**, 744–749.

Neigh, C.S.R., Masek, J.G. & Nickeson, J.E. (2013) High-resolution satellite data open for government research. *Eos, Transactions American Geophysical Union*, **94**, 121–123.

Nowosad, J. & Stepinski, T.F. (2019) Information theory as a consistent framework for quantification and classification of landscape patterns. *Landscape Ecology*, **34**(9), 2091–2101. Available from: https://doi.org/10.1007/s10980-019-00830-x

Olofsson, P., Foody, G.M., Herold, M., Stehman, S.V., Woodcock, C.E. & Wulder, M.A. (2014) Good practices for estimating area and assessing accuracy of land change. *Remote Sensing of Environment*, **148**, 42–57.

Osland, M.J., Chivoiu, B., Enwright, N.M., Thorne, K.M., Guntenspergen, G.R., Grace, J.B. et al. (2022) Migration and transformation of coastal wetlands in response to rising seas. *Science Advances*, **8**(26), eabo5174. Available from: https://doi.org/10.1126/sciadv.abo5174

Osland, M.J., Enwright, N.M., Day, R.H., Gabler, C.A., Stagg, C.L. & Grace, J.B. (2016) Beyond just sea-level rise: considering macroclimatic drivers within coastal wetland vulnerability assessments to climate change. *Global Change Biology*, **22**, 1–11.

Osland, M.J., Feher, L.C., Griffith, K.T., Cavanaugh, K.C., Enwright, N.M., Day, R.H. et al. (2017) Climatic controls on the global distribution, abundance, and species richness of mangrove forests. *Ecological Monographs*, **87**, 341–359.

Osland, M.J., Hughes, A.R., Armitage, A.R., Scyphers, S.B., Cebrian, J., Swinea, S.H. et al. (2022) The impacts of mangrove range expansion on wetland ecosystem services in the southeastern United States: current understanding, knowledge gaps, and emerging research needs. *Global Change Biology*, **28**, 3163–3187.

Patton, D.R. (1975) A diversity index for quantifying habitat "Edge". *Wildlife Society Bulletin (1973–2006)*, **3**, 171–173.

Peterson, J.M. & Bell, S.S. (2012) Tidal events and salt-marsh structure influence black mangrove (*Avicennia germinans*) recruitment across an ecotone. *Ecology*, **93**, 1648–1658.

Peterson, J.M. & Bell, S.S. (2015) Saltmarsh boundary modulates dispersal of mangrove propagules: implications for mangrove migration with sea-level rise. *PLoS One*, **10**, e0119128.

Prener, C., Grossenbacher, T. & Zehr, A. (2022) biscale: tools and palettes for bivariate thematic mapping.

QGIS Development Team. (2023) "QGIS Geographic Information System. Open Source Geospatial Foundation Project". Available from: http://qgis.osgeo.org

Quisthoudt, K., Schmitz, N., Randin, C.F., Dahdouh-Guebas, F., Robert, E.M.R. & Koedam, N. (2012) Temperature variation among mangrove latitudinal range limits worldwide. *Trees*, **26**, 1919–1931.

Richards, D.R., Thompson, B.S. & Wijedasa, L. (2020) Quantifying net loss of global mangrove carbon stocks from 20 years of land cover change. *Nature Communications*, **11**, 4260.

Risser, P.G. (1995) The status of the science examining ecotones: a dynamic aspect of landscape is the area of steep gradients between more homogeneous vegetation associations. *Bioscience*, **45**, 318–325.

Rodriguez, W., Feller, I.C. & Cavanaugh, K.C. (2016) Spatio-temporal changes of a mangrove–saltmarsh ecotone in the northeastern coast of Florida, USA. *Global Ecology and Conservation*, **7**, 245–261.

Rouse, J., Haas, R., Schell, J. & Deering, D. (1974) Monitoring vegetation systems in the Great Plains with ERTS. *NASA Spec. Publ.*, **351**, 309.

Saintilan, N., Wilson, N.C., Rogers, K., Rajkaran, A. & Krauss, K.W. (2014) Mangrove expansion and salt marsh decline at mangrove poleward limits. *Global Change Biology*, **20**, 147–157.

Samworth, R.J. (2012) Optimal weighted nearest neighbour classifiers. *The Annals of Statistics*, **40**, 2733–2763.

Sanderman, J., Hengl, T., Fiske, G., Solvik, K., Adame, M.F., Benson, L. et al. (2018) A global map of mangrove forest soil carbon at 30\hspace0.167emm spatial resolution. *Environmental Research Letters*, **13**, 055002.

Schumaker, N.H. (1996) Using landscape indices to predict habitat connectivity. *Ecology*, **77**, 1210–1225.
Simard, M., Fatoyinbo, L., Smetanka, C., Rivera-Monroy, V.H., Castañeda-Moya, E., Thomas, N. et al. (2019) Mangrove canopy height globally related to precipitation, temperature and cyclone frequency. *Nature Geoscience*, **12**, 40–45.
Simpson, L.T., Cherry, J.A., Smith, R.S. & Feller, I.C. (2021) Mangrove encroachment alters decomposition rate in saltmarsh through changes in litter quality. *Ecosystems*, **24**, 840–854.
Simpson, L.T., Stein, C.M., Osborne, T.Z. & Feller, I.C. (2019) Mangroves dramatically increase carbon storage after 3 years of encroachment. *Hydrobiologia*, **834**, 13–26.
Smith, T.J., Foster, A.M., Tiling-Range, G. & Jones, J.W. (2013) Dynamics of mangrove-marsh ecotones in subtropical coastal wetlands: fire, sea-level rise, and water levels. *Fire Ecology*, **9**, 66–77.
Steinmuller, H.E., Breithaupt, J.L., Engelbert, K.M., Assavapanuvat, P. & Bianchi, T.S. (2022) Coastal wetland soil carbon storage at mangrove range limits in Apalachicola Bay, FL: observations and expectations. *Frontiers in Forests and Global Change*, **5**, 852910.
Talukdar, S., Singha, P., Mahato, S., Shahfahad, Pal, S., Liou, Y.-A. & Rahman, A. (2020) Land-use land-cover classification by machine learning classifiers for satellite observations—a review. *Remote Sensing*, **12**, 1135.
Thomas, N., Bunting, P., Lucas, R., Hardy, A., Rosenqvist, A. & Fatoyinbo, T. (2018) Mapping mangrove extent and change: a globally applicable approach. *Remote Sensing*, **10**, 1466.
Thomas, N., Lucas, R., Bunting, P., Hardy, A., Rosenqvist, A. & Simard, M. (2017) Distribution and drivers of global mangrove forest change, 1996-2010. *PLoS One*, **12**, e0179302.
Tran, T.V., Reef, R. & Zhu, X. (2022) A review of spectral indices for mangrove remote sensing. *Remote Sensing*, **14**, 4868.
Turner, M.G. (1990) Spatial and temporal analysis of landscape patterns. *Landscape Ecology*, **4**, 21–30.
Turner, M.G. & Gardner, R.H. (2015) *Landscape ecology in theory and practice: pattern and process*. New York, NY: Springer.
Turner, M.G. & Ruscher, C.L. (1988) Changes in landscape patterns in Georgia, USA. *Landscape Ecology*, **1**, 241–251.
Turpie, K.R., Klemas, V.V., Byrd, K., Kelly, M. & Jo, Y.-H. (2015) Prospective HyspIRI global observations of tidal wetlands. *Remote Sensing of Environment*, **167**, 206–217.
Uuemaa, E., Mander, Ü. & Marja, R. (2013) Trends in the use of landscape spatial metrics as landscape indicators: a review. *Ecological Indicators*, **28**, 100–106.
Vaughn, D.R., Bianchi, T.S., Shields, M.R., Kenney, W.F. & Osborne, T.Z. (2020) Increased organic carbon burial in northern Florida mangrove-salt marsh transition zones. *Global Biogeochemical Cycles*, **34**, e2019GB006334.
Verutes, G.M., Yang, P.F., Eastman, S.F., Doughty, C.L., Adgie, T.E., Dietz, K. et al. (2024) Using vulnerability assessment to characterize coastal protection benefits provided by estuarine habitats of a dynamic intracoastal waterway. *PeerJ*, **12**, e16738. Available from: https://doi.org/10.7717/peerj.16738
Ximenes, A.C., Cavanaugh, K.C., Arvor, D., Murdiyarso, D., Thomas, N., Arcoverde, G. et al. (2022) A comparison of global mangrove maps: assessing spatial and bioclimatic discrepancies at poleward range limits. *Science of the Total Environment*, **860**, 160380.
Yando, E.S., Jones, S.F. & Hester, M.W. (2021) Limited mangrove propagule retention at a latitudinal Range limit: spatiotemporal patterns at the patch scale. *Estuaries and Coasts*, **44**, 834–845.
Yando, E.S., Osland, M.J. & Hester, M.W. (2018) Microspatial ecotone dynamics at a shifting range limit: plant–soil variation across salt marsh–mangrove interfaces. *Oecologia*, **187**, 319–331.
Yando, E.S., Osland, M.J., Willis, J.M., Day, R.H., Krauss, K.W. & Hester, M.W. (2016) Salt marsh-mangrove ecotones: using structural gradients to investigate the effects of woody plant encroachment on plant-soil interactions and ecosystem carbon pools. *Journal of Ecology*, **104**, 1020–1031.
Yin, F., Lewis, P., Gomez-Dans, J. & Wu, Q. (2019) A sensor-invariant atmospheric correction method: application to Sentinel-2/MSI and Landsat 8/OLI.

Supporting Information

Additional supporting information may be found online in the Supporting Information section at the end of the article.

Table S1. The characteristics of Landsat 8, Sentinel-2, PlanetScope SuperDove, and Worldview-2.
Table S2. Comparison of classification model accuracy among imagery. Model accuracy metrics (accuracy, F-measure, Kappa Coefficient, precision, recall, area under ROC curve, and spec) for Neural Net, K-nn, XGBoost, and Random Forest classification algorithms applied to WorldView, Planet, Sentinel, and Landsat Images.
Table S3. Class Confusion Matrix – Results from the Classification Model Accuracy Assessment using 10-fold cross-validation training-testing split. Note: these differ from the map accuracy assessment.
Table S4. Landcover metrics at the landscape, class, and patch scale. Reported values for classes and patches are means ± SD. Note that only the mangrove class was present for Landsat.